AIAA JOURNAL
Vol. 43, No. 9, September 2005

Flutter and Thermal Deflection Suppression of Composite Plates Using Shape Memory Alloy

Bin Duan*
Claritas, Inc., Arlington, Virginia 22209
Khaled Abdel-Motagaly†
Titan Systems Corporation, Houston, Texas 77058
and
Xinyun Guo‡ and Chuh Mei§
Old Dominion University, Norfolk, Virginia 23529

An efficient finite element method for predicting critical temperature, postbuckling deflection and flutter response is developed for composite plates embedded with prestrained shape memory alloy (SMA) fibers. The large panel deflection and the temperature-dependent material properties of SMA and composites are considered in the formulation. The finite element formulation and solution procedure of the incremental updated Lagrangian method for nonlinear temperature-dependent material properties are presented briefly. Flow yaw angle at supersonic speed is also considered. For the static solution, the system equations are solved by using the Newton–Raphson iteration method to determine aerothermal postbuckling deflection under the combined aerodynamic and thermal loads. For the dynamic flutter response, the modal method and time-domain numerical integration are employed. Results show that the critical buckling temperature can be raised high enough so that buckling deflection can be eliminated, and the desired flat and stable region in the temperature–dynamic pressure operating domain can be enlarged greatly for composite surface panels embedded with SMA for supersonic vehicle applications. Weight savings based on critical temperature when SMA is used are also presented.

Nomenclature

A_s, A_f	=	austenite start and finish temperatures
$[A]$, $[B]$, $[D]$	=	in-plane, coupling and bending laminate stiffness matrices
$[A_a]$	=	aerodynamic influence matrices
C_a	=	aerodynamic damping coefficient
E	=	Young's modulus
$[G]$	=	aerodynamic damping matrix
$[\bar{G}]$	=	modal aerodynamic damping matrix
g_a	=	nondimensional aerodynamic damping
h	=	plate thickness
$[K]$	=	stiffness matrix
$[K_{\text{lin}}]$, $[K^*_{\text{lin}}]$	=	linear stiffness matrices
$[K_1]$, $[K_{10}]$	=	first-order nonlinear stiffness matrices due to large deflection and initial displacement
$[K_2]$	=	second-order nonlinear stiffness matrix due to large deflection
$[\bar{K}]$	=	modal linear stiffness matrix
$[\bar{K}_q]$, $[\bar{K}_{qq}]$	=	modal nonlinear stiffness matrices
$[K^*_1]$, $[K^*_2]$	=	first-order and second-order nonlinear bending stiffness matrices
$[M]$	=	mass matrix
$[\bar{M}_b]$	=	modal bending mass matrix
$\{N\}$, $\{M\}$	=	force and moment vectors
$[N_1]$, $[N_{10}]$	=	first-order nonlinear incremental stiffness matrices due to large deflection and initial displacement
$[N_2]$	=	second-order nonlinear incremental stiffness matrix due to large deflection
P_a	=	aerodynamic pressure
$\{\bar{P}\}$	=	modal force vector
$[Q]$	=	lamina reduced stiffness matrix
$[\bar{Q}]$	=	transformed lamina reduced stiffness matrix
q	=	dynamic pressure/modal coordinate
T	=	temperature
u, v	=	incremental in-plane displacements
u_0, v_0	=	updated initial in-plane displacements
v_s, v_m	=	volume fractions of shape memory alloy (SMA) and traditional composite matrix
$\{W\}$	=	incremental nodal displacement vector
$\{W\}_s$	=	incremental aerothermal nodal displacement vector
$\{W\}_t$	=	dynamic nodal displacement vector
$\{W\}_0$	=	updated initial nodal displacement vector
w	=	incremental transverse displacement
w_0	=	updated initial transverse displacement
x, y, z	=	Cartesian coordinates
α	=	thermal expansion coefficient
ΔT	=	temperature increment
$\{\varepsilon\}$	=	strain vector
$\{\kappa\}$	=	bending curvature vector
Λ	=	flow yaw angle
λ	=	nondimensional dynamic pressure
μ	=	air-panel mass ratio
ρ	=	mass density
$\{\sigma\}$	=	stress vector
$[\Phi]$	=	eigenvector matrix
$\{\phi_i\}$	=	eigenvector

Subscripts

b	=	bending
cr	=	critical

Presented as Paper 2003-1513 at the 44th Structures, Structural Dynamics, and Materials Conference, Norfolk, VA, 7–10 April 2003; received 23 April 2003; revision received 1 July 2004; accepted for publication 29 April 2005.

*Engineer.
†Engineer, Astronautics Engineering Unit.
‡Graduate Research Assistant, Department of Aerospace Engineering; xguo@odu.edu. Student Member AIAA.
§Professor, Department of Aerospace Engineering. Associate Fellow AIAA.

m	=	membrane/composite matrix
NB	=	stiffness matrices due to $\{N_b\}$
Nm	=	stiffness matrices due to $\{N_m\}$
$N\Delta T$	=	stiffness matrices due to $\{N_{\Delta T}\}$
r	=	recovery stress of SMA
s	=	static/quantity related to SMA
t	=	time dependent
ΔT	=	thermal
λ	=	aerodynamic load
σ	=	stress
0	=	initial

Introduction

BECAUSE of aerodynamic heating, surface panels of high-speed vehicles are subjected to temperature that can reach several hundred degrees, for example, 350°F or 177°C for the Quiet Supersonic Platform[1] (QSP) and the High Speed Civil Transport cruising at Mach 2.4. Large thermal deflections of the skin panels may occur. This would alter the vehicle's configuration and affect its aerodynamic characteristics, leading to poor flight performance. Therefore, it is desirable to have a means to suppress the thermal deflection and the flutter response of surface panels under combined thermal and aerodynamic loads.

To reduce the large thermal deflection of surface panels for the X-33, a rugged superalloy thermal protection system (TPS) with overlapping seals has been developed. The titanium honeycomb sandwich TPS was designed to be rather stiff to keep the thermal deflection to a minimum. Chen and Blosser[2] and Cheng et al.[3] have studies the flutter of TPS and thin overlapping inconel seals, respectively.

SMA has a unique ability to recover large prestrains, for example, up to 8–10% elongation for nitinol, completely when the alloy is heated (by the aerodynamic heating in the present case) above the austenite finish temperature A_f. Buehler and Wang[4] found that the austenite start temperature A_s for nitinol (named for nickel, titanium, and the Naval Ordinance Laboratory) can be set anywhere between $-60(-50)$ and $+340$°F ($+170$°C) by varying the nickel content. During the recovery process, a large recovery tensile stress occurs if the shape memory alloy (SMA) is restrained. Cross et al.[5] determined experimentally the recovery stress of nitinol at various prestrain values and Young's modulus vs temperature shown in Figs. 1 and 2, respectively. Both the recovery stress and Young's modulus of SMA exhibit highly nonlinear temperature-dependent properties.

Active control of buckling using recovery stress of SMA fibers has been considered by many researchers. Baz et al.[6,7] presented experiments on buckling of composite beams embedded with nitinol fibers in resin sleeves. SMA fibers were electrically heated and tensile recovery force brought the buckled beam to the original straight position. In addition, they also showed that nitinol fibers can control flow-induced vibrations of composite beams. Rogers[8] proposed an innovative concept to utilize the large recovery stress by embedding the prestrained SMA in a traditional fiber-reinforced composite laminated panel. The SMA fibers are, thus, restrained and large in-plane tensile forces are induced in the panel at temperatures higher than A_s. The large in-plane forces increase the panel stiffness and the natural frequencies. Recently, researchers have investigated the feasibility of SMA hybrid composites (SMAHC) and studied their various applications.[9,10] Turner[11,12] did experiments on thermal postbuckling and random response of SMAHC. The fundamental frequency was shown to increase by a factor of about five, and rms displacement response was attenuated by a factor of 6.4 for a SMAHC beam. A finite element model was developed based on a constitutive model by making use of testing parameters of basic engineering properties of SMA, rather than complex qualitative microstructural constitutive model. Predicted and measured results agreed very well.[11,12]

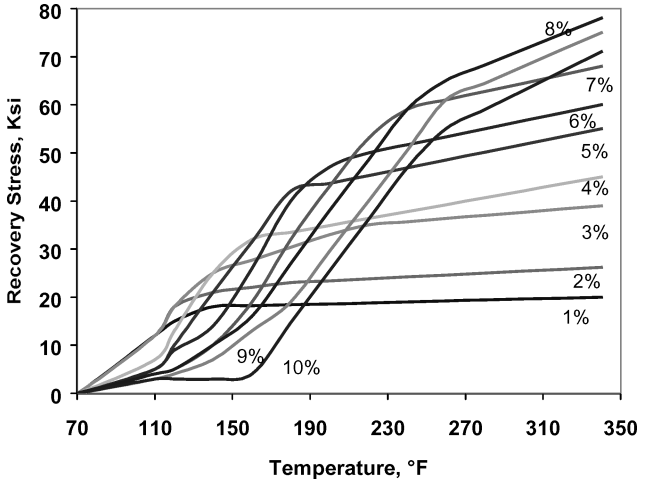

Fig. 1 Recovery stress vs temperature at various prestrains for nitinol.[5]

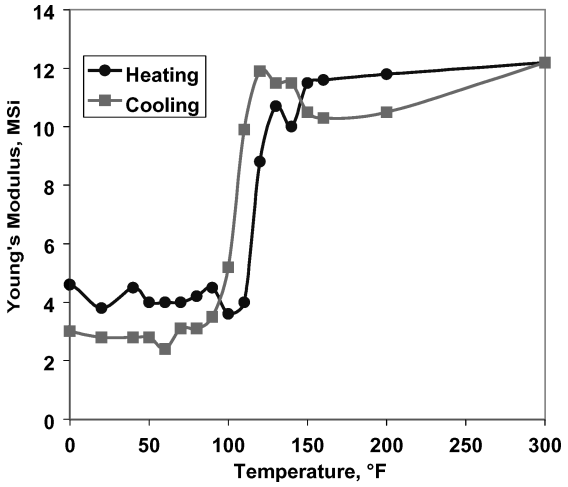

Fig. 2 Elastic modulus and yield stress vs temperature for nitinol.[5]

In two excellent review papers, Thornton[13] and Noor and Burton[14] summarized the effects of temperature-dependent material properties on buckling and postbuckling of plate and shell structures. Kamiya and Fukui[15] investigated the postbuckling of square isotropic plates with temperature-dependent properties. A finite difference method with iteration scheme was used for plates of either simply supported or clamped edges with constrained in-plane displacements. The temperature-dependent properties lower critical temperature, reduce postbuckling stiffness, and increase plate deflection. Chen and Chen[16,17] proposed a finite element method for thermal buckling and postbuckling behavior of laminated composite plates. The temperature-dependent properties lower predictions of critical temperature and reduce thermal postbuckling strength. Noor and Burton[18] studied the effects of temperature-dependent properties on the prebuckling stresses, critical temperatures, and their sensitivity derivatives of antisymmetric angle-ply plates using the three-dimensional thermoelasticity solutions. Numerical results show that the temperature-dependent properties reduce critical temperature and the influence of prebuckling stresses on critical temperature is less significant for the temperature-dependent than the temperature-independent property case. Lee et al.[19] studied the thermal effect with the material degradation on the buckling, vibration, and flutter characteristics of stiffened composite plates using the finite element method. Their results indicate that the material degradation decreases the critical temperature and increases the postbuckling deflection. Note that the mentioned temperature-dependent material properties[15–19] are all assumed to be linear functions of the temperature.

The thermal deflection analysis method for SMA embedded hybrid composites has to consider both nonlinear temperature-dependent material properties and nonlinear large deflections.

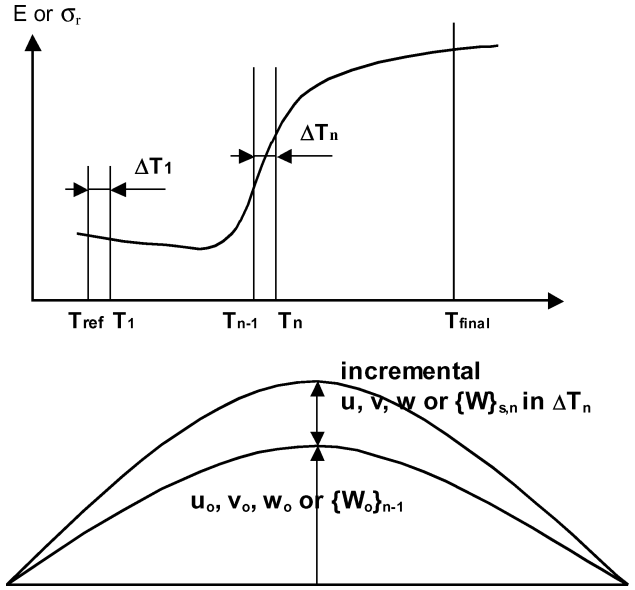

Fig. 3 Schematic of the temperature increment solution procedure.

Mei et al.,[20] and Duan et al.,[21] and Duan[22] introduced an incremental updated Lagrangian finite element method (IUL/FEM). The IUL/FEM method considers 1) small temperature increment ΔT for nonlinear temperature-dependent properties, 2) the prebuckling stresses, and 3) the influence of initial deflection and stresses. In addition, 4) within each increment ΔT, the incremental deflection and stresses are determined by treating the material properties as constant and 5) the initial deflection and stresses are updated with the incremental deflection and stresses and are used for the next increment. The process is repeated until the desired final temperature is reached as shown in Fig. 3.

Before the investigation of suppression of nonlinear supersonic flutter using SMA, panel flutter analysis is briefly reviewed here. Dowell[23] investigated the panel flutter using a partial differential equation Galerkin method and time-domain integration. Mei et al.[24] stated that the finite element modal method and time-domain numerical integration could be employed for the large-amplitude flutter response. Both Dowell and Mei et al. employed the quasi-steady first-order piston theory for the aerodynamic pressure at supersonic speed. Selvam et al.[25] showed that the flutter limit-cycle oscillations (LCO) compared well between the first-order piston theory and the unsteady compressible three-dimensional Euler equations.

Few investigations on nonlinear panel flutter have dealt with yawed airflow. Friedmann and Hanin[26] were the first to study nonlinear flutter of simply supported rectangular isotropic or orthotropic panels with arbitrary supersonic flow directions. They used the first-order quasi-steady aerodynamic theory and Galerkin's method with a 4×2 or eight-mode model. Numerical integration was employed for the LCO response. Chandiramani et al.[27,28] used the third-order piston theory aerodynamics and the higher-order shear deformation theory and investigated nonperiodic flutter of a buckled simply supported composite panel with yawing of flow. Galerkin's method with a 2×2 or four-mode model was employed. For arbitrary laminated anisotropic composite rectangular plates, Abdel-Motagaly et al.[29] have shown that 16 or more modes of the lowest natural frequencies are needed for accurate LCO prediction even at zero yaw angle.

One of the advantages of using SMA to suppress thermal buckling and flutter for surface panels of supersonic vehicles is that the aerodynamic heating is inevitable and, thus, "free" for the activation of SMA fibers. In this paper, the improved IUL/FEM method is presented for predicting critical temperature, postbuckling deflection, and flutter response in consideration of flow yaw angle for symmetrically laminated composite plates embedded with prestrained SMA fibers. The large deflection and the temperature-dependent material properties of both SMA and composites are considered in the formulation. Prebuckling stresses is considered as well because it is an incremental method. The solution procedure consists of two steps: the static/particular solution and the dynamic/homogeneous solution. For the static solution, the system equations are solved using Newton–Raphson iteration method to obtain aerothermal postbuckling deflection. For the dynamic solution, the finite element modal method and time-domain numerical integration are employed to obtain large-amplitude flutter response. Results showed many great advantages in using SMA. First, the critical buckling temperature T_{cr} can be increased. When the design parameters of SMA are varied, T_{cr} can be raised higher than the temperature experienced by the panel from aerodynamic heating ($T_{cr} > 350°$F or 177°C for QSP); thus, the panel thermal postbuckling can be completely suppressed. Second, the critical dynamic pressure λ_{cr} also is increased at high temperatures and the panel flutter response due to dynamic pressure is reduced or suppressed. The flat and stable region for a composite plate embedded with SMA is enlarged greatly. Therefore, the vehicle's highly efficient aerodynamic configuration is maintained, and the vehicle's service life is enhanced due to a lower state of thermal stress and cyclic dynamic stress. The weight saving based on critical temperature in using SMA is also presented.

Equation of Motion in Structural Node Degrees of Freedom

The equations of motion with the consideration of large deflection and nonlinear material properties are formulated for a thin (length/thickness >50) symmetric laminated composite plate embedded with SMA subjected to aerodynamic and thermal loads. When von Kármán moderate large-deflection theory and classical laminated plate theory are used, the incremental strain–displacement relations can be expressed as

$$\{\varepsilon\} = \{\varepsilon^0\} + z\{\kappa\} + \{\varepsilon_0\} = \left\{\varepsilon_m^0\right\} + \left\{\varepsilon_\theta^0\right\} + z\{\kappa\} + \{\varepsilon_0\}$$

$$= \begin{Bmatrix} u_{,x} \\ v_{,y} \\ u_{,y} + v_{,x} \end{Bmatrix} + \frac{1}{2}\begin{Bmatrix} w_{,x}^2 \\ w_{,y}^2 \\ 2w_{,x}w_{,y} \end{Bmatrix} + z\begin{Bmatrix} -w_{,xx} \\ -w_{,yy} \\ -2w_{,xy} \end{Bmatrix}$$

$$+ \begin{Bmatrix} w_{,x}w_{0,x} \\ w_{,y}w_{0,y} \\ w_{,x}w_{0,y} + w_{,y}w_{0,x} \end{Bmatrix} \tag{1}$$

where $\{\varepsilon^0\}$ and $z\{\kappa\}$ are the membrane and bending strain components; $\{\varepsilon_0\}$ is the initial strain corresponding to the initial displacements u_0, v_0, and w_0; and u, v, and w are the incremental displacements measured from the initial displacements as shown in Fig. 3. The subscripts m, θ, and 0 denote membrane, nonlinear, and initial components, respectively.

When the kth layer of a thin composite laminate embedded with SMA fibers is considered, the incremental stress–strain relations within the small temperature increment ΔT are

$$\{\sigma\}_k - \{\sigma_0\}_k = [\bar{Q}]_k \begin{Bmatrix} \varepsilon_x \\ \varepsilon_y \\ \gamma_{xy} \end{Bmatrix} + \begin{Bmatrix} \sigma_{xr} \\ \sigma_{yr} \\ \tau_{xyr} \end{Bmatrix}_k v_s$$

$$- \left([\bar{Q}_m] \begin{Bmatrix} \alpha_{xm} \\ \alpha_{ym} \\ \alpha_{xym} \end{Bmatrix} v_m \right)_k \Delta T, \qquad T \geq A_s \tag{2}$$

$$\{\sigma\}_k - \{\sigma_0\}_k = [\bar{Q}]_k \left(\begin{Bmatrix} \varepsilon_x \\ \varepsilon_y \\ \gamma_{xy} \end{Bmatrix} - \begin{Bmatrix} \alpha_x \\ \alpha_y \\ \alpha_{xy} \end{Bmatrix}_k \Delta T \right), \qquad T < A_s \tag{3}$$

where subscript k denotes the general kth layer, $\{\sigma\}_k$ is the total stress vector measured from the stress-free state at T_{ref}, and $\{\sigma_0\}_k$ is the initial stress before the current temperature increment ΔT. The vector $\lfloor \boldsymbol{\sigma}_{xr}, \boldsymbol{\sigma}_{yr}, \boldsymbol{\tau}_{xyr} \rfloor_k^T$, which is dependent on the prestrain ε_r as shown in the experimental data[5] in Fig. 1, is the incremental recovery stress vector generated by SMA if temperature is higher than A_s.

At temperature lower than A_s, there is no shape memory effect, and the SMA embedded composite acts as a traditional composites shown in Eq. (3). Matrix $[\bar{Q}]_k$ is the kth layer transformed reduced material stiffness for the composite matrix and SMA fibers based on the rules of material micromechanics, $[\bar{Q}_m]_k$ is the transformed reduced material stiffness for composite matrix only, and v_s and v_m are the volume fractions of SMA and composite matrix, respectively.

The constitutive equations of a laminated composite plate embedded with SMA from Eqs. (2) and (3) can be expressed as

$$\begin{Bmatrix} N \\ M \end{Bmatrix} - \begin{Bmatrix} N_\sigma \\ M_\sigma \end{Bmatrix} = \begin{bmatrix} A & B \\ B & D \end{bmatrix} \begin{Bmatrix} \varepsilon^0 \\ \kappa \end{Bmatrix} - \begin{Bmatrix} N_{\Delta T} \\ M_{\Delta T} \end{Bmatrix} + \begin{Bmatrix} N_r \\ M_r \end{Bmatrix} \tag{4}$$

where $[A]$, $[B]$ and $[D]$ are the laminate extension, extension–bending, and bending stiffness matrices; $\{N_r\}$ and $\{M_r\}$, and $\{N_{\Delta T}\}$ and $\{M_{\Delta T}\}$ are the incremental force and moment vectors, which are due to the incremental SMA recovery stress, and the incremental thermal stress in a temperature increment ΔT, respectively. The resultant force and moment vectors $\{N_\sigma\}$ and $\{M_\sigma\}$ are due to the initial stresses before the current temperature increment.

The quasi-steady first-order theory is employed for the aerodynamic pressure at supersonic speed, $M_\infty > 1.6$. Considering flow yaw angle effect, we have

$$P_a = -\frac{2q}{\beta}\left[\frac{\partial w}{\partial x}\cos(\Lambda) + \frac{\partial w}{\partial y}\sin(\Lambda) + \frac{M_\infty^2 - 2}{M_\infty^2 - 1}\frac{1}{V}\frac{\partial w}{\partial t}\right]$$

$$= -\left[\lambda\frac{D_{110}}{L^3}\left(\frac{\partial w}{\partial x}\cos(\Lambda) + \frac{\partial w}{\partial y}\sin(\Lambda)\right) + \frac{g_a}{\omega_0}\frac{D_{110}}{L^4}\frac{\partial w}{\partial t}\right] \tag{5}$$

where V is the airflow velocity, M_∞ is the Mach number, $q = \frac{1}{2}\rho_a V^2$ is the dynamic pressure, ρ_a is the air mass density, $\beta = \sqrt{(M_\infty^2 - 1)}$, w is the panel transverse displacement, D_{110} is the first entry in the laminate bending stiffness matrix $[D]$ calculated when assuming all of the fibers of the composite layers are aligned in the x direction, and L is the panel length. The nondimensional dynamic pressure λ and aerodynamic damping g_a are

$$\lambda = \frac{2qL^3}{\beta D_{110}}, \qquad g_a = \frac{\rho_a V\left(M_\infty^2 - 2\right)}{\beta^3 \rho h \omega_0} = \sqrt{\lambda C_a} \tag{6}$$

The aerodynamic damping coefficient C_a and mass ratio μ are

$$C_a = \left[\left(M_\infty^2 - 2\right)^2 \Big/ \beta^5\right]\mu, \qquad \mu = \rho_a L/\rho h \tag{7}$$

For $M_\infty \gg 1$, $C_a \approx \mu/M_\infty$.

To derive the equations of motion in a finite element, the principle of virtual work is employed as

$$\delta W = \delta W_{\text{int}} - \delta W_{\text{ext}} = 0 \tag{8}$$

where the virtual work of the internal forces on a plate element is given by

$$\delta W_{\text{int}} = \int_A \left(\{\delta\varepsilon^0\}^T\{N\} + \{\delta\kappa\}^T\{M\}\right) \mathrm{d}A \tag{9}$$

and the virtual work of the external forces on a plate element, considering inertia, and aerodynamic and random excitations, is

$$\delta W_{\text{ext}} = \int_A \{\delta w[-\rho h\ddot{w} + P_a + P(t)] + \delta u(-\rho h\ddot{u}) + \delta v(-\rho h\ddot{v})\} \mathrm{d}A \tag{10}$$

After a long and tedious derivation, the system equation of motion can be obtained as[22]

$$\begin{bmatrix} M_b & 0 \\ 0 & M_m \end{bmatrix}\begin{Bmatrix} \ddot{W}_b \\ \ddot{W}_m \end{Bmatrix} + g_a\begin{bmatrix} G & 0 \\ 0 & 0 \end{bmatrix}\begin{Bmatrix} \dot{W}_b \\ \dot{W}_m \end{Bmatrix} + \left(\lambda\begin{bmatrix} A_a(\Lambda) & 0 \\ 0 & 0 \end{bmatrix} + \begin{bmatrix} K_b & 0 \\ 0 & K_m \end{bmatrix} + \begin{bmatrix} K_{0b} & K_{0bm} \\ K_{0mb} & 0 \end{bmatrix} - \begin{bmatrix} K_{N\Delta Tb} & 0 \\ 0 & 0 \end{bmatrix} + \begin{bmatrix} K_{rb} & 0 \\ 0 & 0 \end{bmatrix} + \begin{bmatrix} K_{\sigma b} & 0 \\ 0 & 0 \end{bmatrix} + \frac{1}{2}\begin{bmatrix} N_{1Nm} & N_{1bm} \\ N_{1mb} & 0 \end{bmatrix} + \frac{1}{2}\begin{bmatrix} N_{10b} & 0 \\ 0 & 0 \end{bmatrix} + \frac{1}{3}\begin{bmatrix} N_{2b} & 0 \\ 0 & 0 \end{bmatrix}\right)\begin{Bmatrix} W_b \\ W_m \end{Bmatrix} = \begin{Bmatrix} P_{\Delta Tb} \\ P_{\Delta Tm} \end{Bmatrix} - \begin{Bmatrix} P_{\sigma b} \\ P_{\sigma m} \end{Bmatrix} - \begin{Bmatrix} P_{rb} \\ P_{rm} \end{Bmatrix} - \begin{Bmatrix} P_{\lambda 0b} \\ 0 \end{Bmatrix} \tag{11}$$

or simply

$$[M]\{\ddot{W}\} + g_a[G]\{\dot{W}\} + \left(\lambda[A_a(\Lambda)] + [K] + [K_0] - [K_{N\Delta T}] + [K_r] + [K_\sigma] + \tfrac{1}{2}[N_1] + \tfrac{1}{2}[N_{10}] + \tfrac{1}{3}[N_2]\right)\{W\} = \{P_{\Delta T}\} - \{P_\sigma\} - \{P_r\} - \{P_{\lambda 0}\} \tag{12}$$

where $\{W_b\}$ and $\{W_m\}$ are the nodal incremental bending and membrane displacement vectors, which are measured from the initial displacement vector $\{W\}_0$; $[M]$, $[G]$, and $[K]$ are mass, aerodynamic damping, and linear stiffness matrices, respectively; $[K_0]$ is the linear stiffness matrix due to the initial displacement; $[A_a]$, and $[K_{N\Delta T}]$ and $[K_r]$ are the aerodynamic influence and geometric stiffness matrices due to $\{N_{\Delta T}\}$ and $\{N_r\}$, respectively; $[N_1]$, $[N_{10}]$, and $[N_2]$ are the nonlinear incremental stiffness matrices, which are linearly and quadratically dependent on incremental displacement vector $\{W\}$; $[N_{10}]$ also depends on known initial displacement vector $\{W\}_0$; and $\{P_{\Delta T}\}$, $\{P_\sigma\}$, $\{P_r\}$, and $\{P_{\lambda 0}\}$ are load vectors due to temperature, initial stress, recovery stress, and coupling of dynamic pressure and initial displacement, respectively. The models of increased stiffness in beams and plates using SMA have been verified experimentally by various investigators,[6,7,11,12] and Turner[12] used a model similar to Eq. (12) to predict the frequency response of a SMAHC beam accurately.

Solution Procedures

The solution of differential equation (12) with steady-state forcing terms can be considered as the summation of a time-independent particular solution and a time-dependent homogenous solution as

$$\{W\} = \{W\}_s + \{W\}_t \tag{13}$$

where $\{W\}_s$ is the incremental aerothermal displacement (time-independent particular solution) and $\{W\}_t$ is the self-excited dynamic oscillations (time-dependent homogenous solution) about the aerothermally deformed equilibrium position. The vector $\{W\}_s$ is an incremental quantity in the sense that it is the static displacement during a incremental temperature ΔT_n or $(T_n - T_{n-1})$. The amplitude of $\{W\}_s$ is not necessarily small. The vector $\{W\}_t$ is the dynamic displacement response at a particular temperature T, and similarly it is not necessarily small. Notice that only $\{W\}_s$ is used to update the initial displacement $\{W\}_0$ for the next temperature increment ΔT_{n+1}.

When Eq. (13) is substituted into Eq. (12), it can be separated into two equations,

$$\left(\lambda[A_a(\lambda)] + [K_{\text{lin}}] + \tfrac{1}{2}[N_1]_s + \tfrac{1}{2}[N_{10}]_s + \tfrac{1}{3}[N_2]_s\right)\{W\}_s = \{P_{\Delta T}\} - \{P_\sigma\} - \{P_r\} - \{P_{\lambda 0}\} \tag{14}$$

$$[M]\{\ddot{W}\}_t + g_a[G]\{\dot{W}\}_t + (\lambda[A_a(\Lambda)] + [K_{\text{lin}}] + [K_1]_t + [K_{10}]_t + [K_2]_t)\{W\}_t + ([N_1]_s + [N_{10}]_s + [N_2]_s + [N_2]_{st})\{W\}_t = 0 \tag{15}$$

where $[K_{\text{lin}}]$ is the sum of the linear stiffness matrices ($[K_{\text{lin}}] = [K] + [K_0] - [K_{N\Delta T}] + [K_r] + [K_\sigma]$), and $[K_1] = \frac{1}{2}[N_1]$, $[K_{10}] = \frac{1}{2}[N_{10}]$ and $[K_2] = \frac{1}{3}[N_2]$ are the nonlinear stiffness matrices, respectively. Subscripts s and t denote that the corresponding nonlinear matrix is evaluated by $\{W\}_s$ and $\{W\}_t$, respectively. Equation (14) is a set of nonlinear algebraic equations, and Eq. (15) is a set of nonlinear differential equations. The corresponding solution procedures are given as follows.

Aerothermal and Thermal Postbuckling Deflections

For a given λ, a flow yaw angle Λ, and a final temperature T_{final}, the aerothermal postbuckling deflections $\{W\}_s$ is solved from Eq. (14) by using the IUL and Newton–Raphson iteration methods. The temperature range between T_{ref} and T_{final} is divided into many small increments ΔT_n (Fig. 3). At T_{ref}, the SMA embedded composite plate is in a stress-free state (zero initial displacement and initial stresses). In each ΔT_n, the material properties are approximated as constants and the incremental displacement is solved from Eq. (14) by using the Newton–Raphson iteration method. The total deflection is then obtained by adding the incremental displacement to the initial displacement from the previous calculation. The initial displacement and initial stresses are updated, and the next ΔT_n is introduced. The procedure is repeated until T_{final} is reached. The traditional thermal postbuckling is a special case of aerothermal postbuckling deflection by setting $\lambda = 0$ in Eq. (14). The temperature is recorded as critical buckling temperature T_{cr} when the largest element of transverse component in the total displacement vector becomes comparable ($>0.1h$) with the plate thickness h for the first time.

Once the static incremental thermal postbuckling $\{W\}_s$ is obtained, the linear vibration frequency of the thermally buckled plate at this new equilibrium position ($\{W\}_0 + \{W\}_s$) can be determined by neglecting the damping term and the nonlinear stiffness matrices containing $\{W\}_t$ in Eq. (15) as

$$[M]\{\ddot{W}\}_t + ([K_{\text{lin}}] + [N_1]_s + [N_{10}]_s + [N_2]_s)\{W\}_t = 0 \tag{16}$$

Equation (16) is then solved as a standard linear eigenvalue problem to obtain the linear frequencies and mode shapes. The linear frequency about the deformed or buckled equilibrium position is helpful in the explanation of the influence of SMA on the panel response.

Dynamic Panel Response

After the initial nodal static displacement vector $\{W\}_0$ and the static incremental displacement $\{W\}_s$ are obtained, Eq. (15) can be solved to obtain the system dynamic response $\{W\}_t$ at that particular temperature. When the in-plane inertia term is neglected, $\{W_m\}_t$ can be expressed in terms of $\{W_b\}_t$ as

$$\{W_m\}_t = -[K_m]^{-1}([K_{0mb}] + [K_{1mb}]_t + [N_{1mb}]_s)\{W_b\}_t \tag{17}$$

Equation (15) can then be transferred to

$$[M_b]\{\ddot{W}_b\}_t + g_a[G]\{\dot{W}_b\}_t + \left(\left[K^*_{\text{lin}}\right] + \left[K^*_1\right] + \left[K^*_2\right]\right)\{W_b\}_t = 0 \tag{18}$$

where

$$\begin{aligned}\left[K^*_{\text{lin}}\right] &= \lambda[A_a] + [K_b] + [K_{0b}] - [K_{N\Delta Tb}] + [K_{rb}] + [K_{\sigma b}] \\ &\quad + [N_{1Nm}]_s + [N_{10b}]_s + [N_{2b}]_s - ([K_{0bm}] \\ &\quad + [N_{1bm}]_s)[K_m]^{-1}([K_{0mb}] + [N_{1mb}]_s)\end{aligned} \tag{19}$$

is the combined linear stiffness matrix that contains constant matrices and matrices due to known aerothermal displacement vectors $\{W_b\}_s$ and $\{W_m\}_s$ and

$$\begin{aligned}\left[K^*_1\right] &= [K_{1Nm}]_t + [K_{10b}]_t + [N_{2b}]_{st} - [K_{1bm}]_t[K_m]^{-1}([K_{0mb}] \\ &\quad + [N_{1mb}]_s) - ([K_{0bm}] + [N_{1bm}]_s)[K_m]^{-1}[K_{1mb}]_t\end{aligned} \tag{20}$$

$$\left[K^*_2\right] = [K_{2b}]_t - [K_{2Nm}]_t - [K_{1bm}]_t[K_m]^{-1}[K_{1mb}]_t \tag{21}$$

are the combined nonlinear stiffness matrices, which are linearly and quadratically dependent on bending displacement vector $\{W_b\}_t$, respectively.

The bending displacement vector $\{W_b\}_t$ can be expressed as a linear combination of some known base functions (modal transformation) as

$$\{W_b\}_t \approx \sum_{i=1}^{n} q_i\{\phi_i\} = [\Phi]\{q\} \tag{22}$$

where q_i is the ith natural coordinate and $\{\phi_i\}$ is the ith mode shape vector, which is determined by solving the eigenvalue problem of the linear free vibration as

$$\omega_i^2[M_b]\{\phi_i\} = [K_b]\{\phi_i\} \tag{23}$$

The system dynamic equation (18) is transformed into the reduced modal coordinates as[22,29]

$$\lfloor\bar{M}_b\rfloor\{\ddot{q}\} + g_a\lfloor\bar{G}\rfloor\{\dot{q}\} + (\lfloor\bar{K}\rfloor + \lfloor\bar{K}_q\rfloor + \lfloor\bar{K}_{qq}\rfloor)\{q\} = 0 \tag{24}$$

where $\lfloor\bar{M}_b\rfloor$,$\lfloor\bar{G}\rfloor$, and $\lfloor\bar{K}\rfloor$are the modal mass, aerodynamic damping, and linear stiffness matrices expressed as

$$(\lfloor\bar{M}_b\rfloor, \lfloor\bar{G}\rfloor, \lfloor\bar{K}\rfloor) = [\Phi]^T\left([M_b], [G], \left[K^*_{\text{lin}}\right]\right)[\Phi] \tag{25}$$

The first-order and second-order nonlinear modal stiffness matrices $\lfloor\bar{K}_q\rfloor$ and $\lfloor\bar{K}_{qq}\rfloor$ are

$$\begin{aligned}[\bar{K}_q] &= [\Phi]^T\sum_{i=1}^{n} q_i\left([K_{1Nm}]_t^{(i)} + [K_{10b}]_t^{(i)} + [N_{2b}]_{st}^{(i)}\right. \\ &\quad - [K_{1bm}]_t^{(i)}[K_m]^{-1}([K_{mb0}] + [N_{1mb}]_s) - ([K_{0bm}] \\ &\quad \left. + [N_{1bm}]_s)[K_m]^{-1}[K_{1mb}]_t^{(i)}\right)[\Phi]\end{aligned} \tag{26}$$

$$\begin{aligned}[\bar{K}_{qq}] &= [\Phi]^T\sum_{i=1}^{n}\sum_{j=1}^{n} q_iq_j\left([K_{2b}]_t^{(i,j)} - [K_{2Nm}]_t^{(i,j)}\right. \\ &\quad \left. - [K_{1bm}]_t^{(i)}[K_m]^{-1}[K_{1mb}]_t^{(j)}\right)[\Phi]\end{aligned} \tag{27}$$

The nonlinear modal matrices $\lfloor\bar{K}_q\rfloor$ and $\lfloor\bar{K}_{qq}\rfloor$ in Eqs. (26) and (27) are functions of the modal coordinate vector $\{q\}$ only.

With a given set of temperature T, dynamic pressure λ, flow yaw angle Λ, and aerodynamic damping coefficient C_a, the modal amplitude $\{q\}$ can be determined from Eq. (24) using any numerical integration scheme such as the Runge–Kutta or Newmark-β method. Runge–Kutta is employed in the present paper. The system node degrees of freedom (DOF) $\{W_b\}_t$ and $\{W_m\}_t$ can be obtained by using Eqs. (22) and (17), respectively. The total displacement response is then obtained as a sum of the three displacements, $\{W\}_0$, $\{W\}_s$, and $\{W\}_t$.

It is known that six in vacuo modes, from (1,1) to (6,1), are needed for converged LCOs of isotropic rectangular plates exposed to supersonic flow at zero yaw angle.[23,24] For isotropic or orthotropic rectangular plates under an arbitrary nonzero yawed supersonic flow, then 36 natural modes, from (1,1) to (6,6), are needed; for laminated anisotropic rectangular plates even at zero yaw angle, 36 or fewer natural modes are needed.[29]

Results and Discussion

The most widely used SMA is nitinol, and it is employed in this study. Nitinol's properties, shown in Figs. 1 and 2, are adopted and modified slightly in this study. A_s of nitinol is set to 70°F (21°C) so that the SMA phase transformation can be activated at the room (reference) temperature. This can be achieved by adjusting the nickel content in nitinol to 55.6% (Ref. 4). A simply supported $12 \times 12 \times 0.05$ in. ($30.5 \times 30.5 \times 0.125$ cm) graphite–epoxy plate of eight layers $[0/-45/45/90]_s$ embedded with SMA is investigated. The material properties of graphite–epoxy are also considered temperature-dependent as listed in Table 1. A titanium plate of the same dimensions and boundary conditions is also considered for comparison, and its properties are also listed in Table 1.

The finite element employed in the examples is an extended[30] four-node Bogner–Fox–Schmit[31] (BFS) rectangular plate element. The BFS element has 24 DOF, 6 at each node; the bending DOF $\{w_b\}$ comprise transverse displacements and first and second derivatives of displacements w, $w_{,x}$, $w_{,y}$, and $w_{,xy}$; and the in-plane DOF $\{w_m\}$ comprise u and v. For the isotropic titanium plate at $\Lambda = 0$, a 12×6 mesh or 72 BFS elements in a half plate model is used. The composite plate is modeled using a full plate with 12×12 mesh or 144 BFS elements for both $\Lambda = 0$ and $\Lambda \neq 0$.

Table 1 Material properties of nitinol, graphite–epoxy lamina, and titanium alloy

Nitinol[a]		Graphite–epoxy		Titanium alloy	
Property	Value	Property	Value	Property	Value
G	3.604×10^6 psi, $T < A_s$	E_1	$22.5 \times 10^6 (1 - 3.53 \times 10^{-4} \cdot \delta T)^b$ psi	E	14.94×10^6 psi
	(24.9 GPa)	E_2	$1.17 \times 10^6 (1 - 4.27 \times 10^{-4} \cdot \delta T)^b$ psi		(103 GPa)
	3.712×10^6 psi, $T \geq A_s$	G_{12}	$0.66 \times 10^6 (1 - 6.06 \times 10^{-4} \cdot \delta T)^b$ psi	μ	0.37
	(25.6 GPa)	μ_{12}	0.22	ρ	0.424×10^{-3} lb $\cdot$ s^2/in.^{4}
ρ	0.6067×10^{-3} lb $\cdot$ s^2/in.^{4}	ρ	0.1458×10^{-3} lb $\cdot$ s^2/in.^{4}		(4510 kg/m^3)
	(6450 kg/m^3)		(1550 kg/m^3)	α	4.78×10^{-6}/°F
μ	0.3	α_1	$-0.04 \times 10^{-6} (1 - 1.25 \times 10^{-3} \cdot \delta T)^b$/°F		
α	5.7×10^{-6}/°F	α_2	$16.7 \times 10^{-6} (1 + 0.41 \times 10^{-4} \cdot \delta T)^b$		
	(10.26×10^{-6}/°C)				

[a]See Figs. 1 and 2 for recovery stresses and Young's modulus. [b]Where $\delta T = T - T_{\text{ref}}$.

Table 2 Critical buckling temperatures T_{cr}, °F (°C)

Plate	Simply supported	Clamped
Titanium	74 (23.3)	80 (26.7)
Graphite–epoxy		
$v_s = 0\%$, $\varepsilon_r = 0\%$	90 (32.2)	108 (42.2)
$v_s = 10\%$, $\varepsilon_r = 3\%$	209 (98.3)	244 (117.8)
$v_s = 10\%$, $\varepsilon_r = 5\%$	339 (170.6)	390 (198.9)
$v_s = 20\%$, $\varepsilon_r = 3\%$	417 (213.9)	473 (245.0)

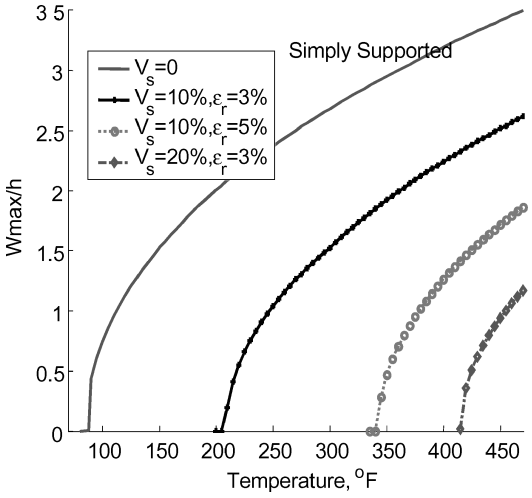

Fig. 4 Maximum thermal deflection of simply supported plates, $\lambda = 0$ and $\Lambda = 0$.

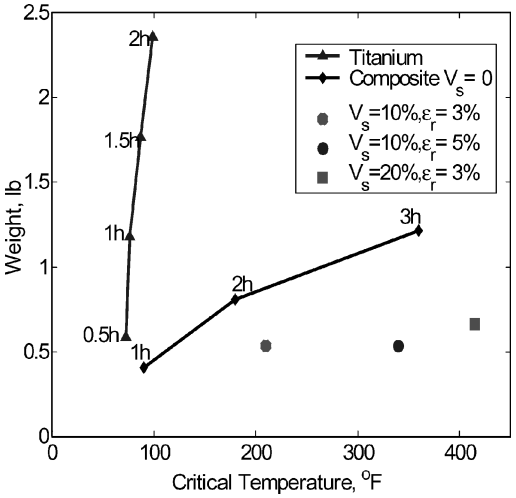

Fig. 5 Plate weight vs T_{cr} for simply supported plates, $h = 0.050$ in., $\lambda = 0$, and $\Lambda = 0$.

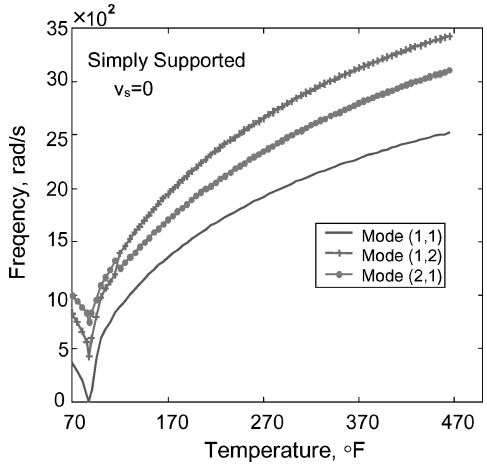

Fig. 6 Linear frequencies vs temperature for a simply supported traditional [0/−45/45/90]$_s$ plate.

Thermal Deflection and Vibration About Buckled Position

The critical temperatures ($\lambda = 0$) for titanium, composite plates with or without SMA are shown in Table 2. It also includes the clamped boundary conditions as comparison. The maximum thermal deflections of the simply supported composite plate with various SMA volume fraction v_s and prestrain ε_r are shown in Fig. 4. Three SMA embedded composite plates from Table 2 have critical buckling temperatures higher than 350°F (177°C). They are 1) the simply supported case with $v_s = 20\%$ and $\varepsilon_r = 3\%$, 2) the clamped case with $v_s = 10\%$ and $\varepsilon_r = 5\%$, and 3) the clamped case with $v_s = 20\%$ and $\varepsilon_r = 3\%$, and they are applicable to QSP for their capability to eliminate the large thermal deflection completely.

The mass density of graphite–epoxy is 1550 kg/m^3. Nitinol and titanium are much heavier. What is the difference in weight for the different plates to have the same critical buckling temperature? The weights for SMA embedded composite plates are compared with traditional composite ($v_s = 0$) and titanium plates and presented in Fig. 5. Dynamic pressure λ is set to zero for this weight-saving calculation. For the traditional composite and titanium plates, the thickness of the plate is varied through a multiple of the base thickness $h = 0.05$ in. (0.125 cm) (for example, $0.5h$ means the thickness is 0.025 in., etc.). It is shown that for a plate to achieve a given T_{cr}, for example, 350°F (177°C), the weight of plate embedded with SMA ($v_s = 10\%$ and $\varepsilon_r = 5\%$) is about 0.66 lb (0.30 kg), whereas the weight is 1.2 lb (0.54 kg) for traditional composite plate of thickness $3h$ (0.15 in.). It is obvious that the weight of titanium plate is the heaviest. It is seen greatly savings can be achieved with the use of SMA.

The lowest three linear frequencies vs temperature at $\lambda = 0$ for traditional composite plate and plate embedded with SMA are shown in Figs. 6 and 7, respectively. The fundamental frequencies for both plates go to zero at T_{cr}. In Fig. 6, the frequencies decrease between

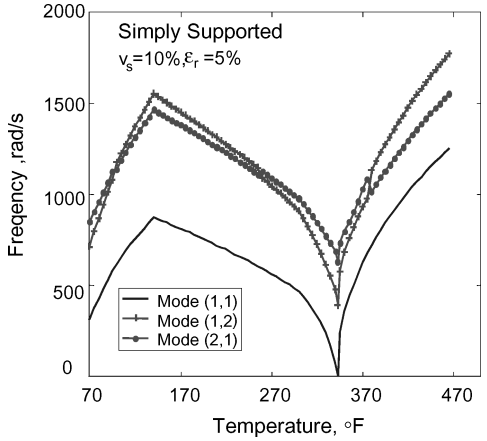

Fig. 7 Linear frequencies vs temperature for a simply supported $[0/-45/45/90]_s$ plate with SMA.

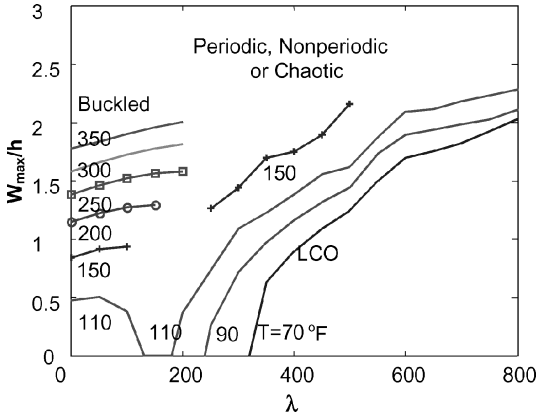

Fig. 8 Aerothermal deflection and LCO amplitude vs dynamic pressure at various temperatures for simply supported $[0/-45/45/90]_s$ plate, $\Lambda = 0$.

T_{ref} and T_{cr} due to the thermal expansion effect. At T_{cr}, the plate loses static stability, and the bifurcation deflection occurs. The frequencies increase after passing T_{cr} because the geometrical nonlinearity contributes stiffness to the plate. There is a modal crossing between modes (1,2) and (2,1) at $T = 120°F$ (49°C). In Fig. 7, the frequencies increase at first, then decrease at the range between T_{ref} through T_{cr}. This is due to the interactions between the SMA recovery stress and the thermal expansion effect. When the temperature is low, the SMA recovery stress overwhelms the thermal expansion effect and makes the plate stiffer. As the temperature increases further, the SMA recovery stress gradually becomes saturated, and the thermal expansion effect gradually dominates.

Aerothermal Deflection and Dynamic Response

With the presence of dynamic pressure, the aerothermal deflection of Eq. (14) becomes complicated. The maximum deflection is no longer located at the plate center. The nature of skew-symmetric $[A_a]$ matrix contributes to the dynamic instability of the system.

After the initial nodal static displacement vector $\{W\}_0$ and the static incremental displacement $\{W\}_s$ are determined for a given temperature, the system dynamic response $\{W\}_t$ is solved numerically through the modal equation (24). For the composite plate, the lowest 36 modes are used for accurate numerical results.

The aerothermal postbuckling deflections and LCO amplitudes vs dynamic pressure (at $\Lambda = 0$) at various temperatures are shown in Fig. 8 for the traditional graphite–epoxy composite panel ($v_s = 0$) with $C_a = 0.05$. The curves on the left side of Fig. 8 are the aerothermal buckled deflections at $T > T_{cr}$, where $T_{cr} = 90°F$ (32°C), and the panel is dynamically stable. The curves on the right-hand side are the LCO amplitudes at different T. At the lower temperature range,

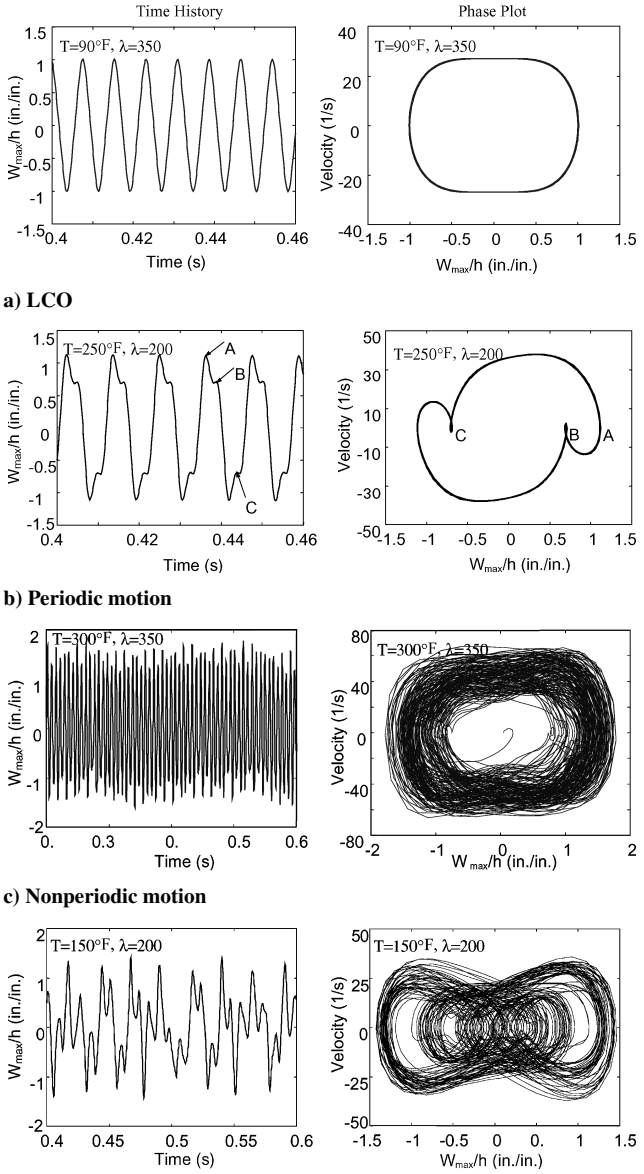

Fig. 9 Time histories and phase plot of LCO, periodic, nonperiodic, and chaotic motions for simply supported traditional $[0/-45/45/90]_s$ plate, $\Lambda = 0$.

$70°F < T < 90°F$ (21°C < T < 32°C), the plate remains flat until λ reaches λ_{cr}, and LCO begins. At the higher temperature range, $90°F < T < 110°F$ (32°C < T < 43°C), the plate first becomes thermally buckled at zero or small λ values; the plate returns to flat and stable state with increasing λ until λ reaches λ_{cr} because the plate is stiffened due to dynamic pressure λ; after $\lambda > \lambda_{cr}$, LCO begins. At $T > 110°F$ (43°C), the plate cannot go back to flat and begins chaotic flutter motions with increasing λ right after being aerothermally buckled. This indicates that the flutter has evolved from nearly simply harmonic LCO to periodic, nonperiodic, or chaotic motion. Figure 9 shows the time histories and phase plots of the four types of motions: LCO at $T = 90°F$ (32°C) and $\lambda = 350$ (Fig. 9a), periodic at $T = 150°F$ (66°C) and $\lambda = 350$ (Fig. 9b), nonperiodic at $T = 250°F$ (121°C) and $\lambda = 500$ (Fig. 9c), and chaos at $T = 150°F$ (66°C) and $\lambda = 200$ (Fig. 9d).

Figure 10 shows aerothermal deflection and LCO amplitudes for the composite plate embedded with SMA of $v_s = 10\%$ and $\varepsilon_r = 3\%$. Compared with Fig. 8, the critical dynamic pressures λ_{cr} at $T = 70°F$ (21°C), 90°F (32°C), and 110°F (43°C) are increased, and the aerothermal buckling at $T = 150°F$ (66°C) and 200 F (93°C) are eliminated due to SMA effects. Note that λ_{cr} at 110°F (43°C)

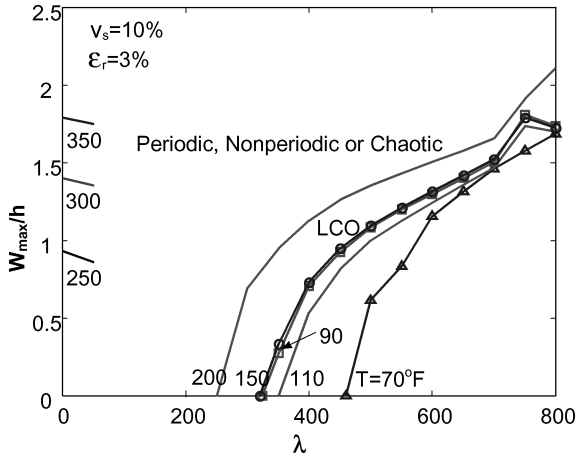

Fig. 10 Aerothermal deflection and LCO amplitude vs dynamic pressure at various temperatures for simply supported $[0/-45/45/90]_s$ plate with SMA, $\Lambda = 0$.

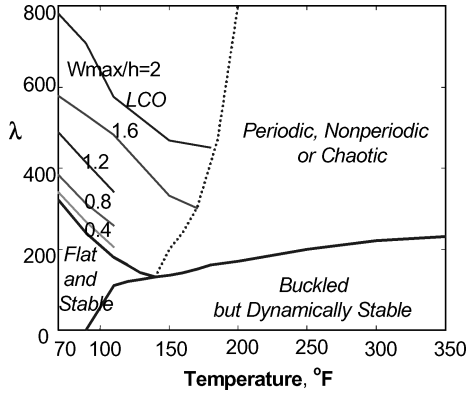

Fig. 11 Stability regions and LCO amplitudes for simply supported traditional $[0/-45/45/90]_s$ plate, $\Lambda = 0$.

is higher than λ_{cr} at 90°F (32°C). This is due to the counteraction between the thermal expansion effect of the composite matrix and the SMA effect. Thermal expansion has the tendency to soften the plate and to reduce λ_{cr}, whereas the SMA recovery stress stiffens the plate and increases λ_{cr}. Between 90°F (32°C) through 110°F (43°C), the SMA effect overcomes the thermal expansion effect, the plate is stiffened, and λ_{cr} is increased. With the further increase of temperature, the thermal expansion effect gradually becomes dominant, and the plate displays the reduced stiffness and reduced λ_{cr}, which is shown for $T = 150$°F (66°C) and 200°F (93°C) in Fig. 10. There are still chaotic oscillations occurring at $T = 250$°F (121°C), 300°F (154°C), and 350°F (177°C) when $\lambda > 50$.

Stability Regions

The stability regions of the traditional composite panel, $v_s = 0$, in the temperature–dynamic pressure ($T \sim \lambda$) domain are shown in Fig. 11 ($\Lambda = 0$, $C_a = 0.05$). There are four regions: flat and stable, buckled but dynamically stable, LCO, and chaos. Among the four regions, a large flat and stable region is desirable, and LCO and chaos are the regions to be averted in design. Limit cycle comprises nearly simply harmonic LCO and periodic LCO. With the increase of T and λ, the nearly simple harmonic LCO has the tendency to evolve to periodic LCO, as mentioned before. The motion map also shows that in some points, especially when T is high, the plate undergoes LCO about the buckled equilibrium position. There are points inside the chaos region, at which the plate undergoes periodic LCO motion. This corresponds to the discovery by Dowell[23] that, even inside the chaos region, there still exist some combinations of system control parameters that lead to periodic motion. Figure 11 also shows lines inside limit-cycle region on which the flutters have the same amplitudes.

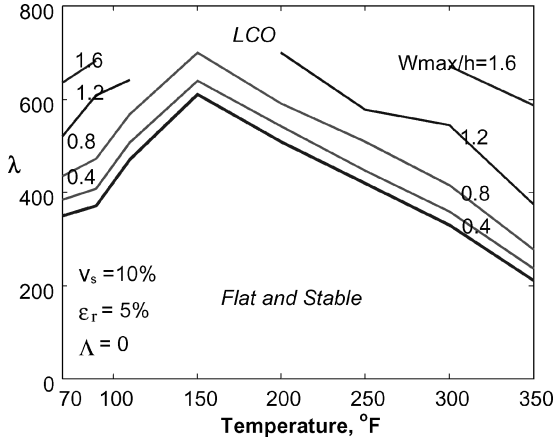

Fig. 12 Stability regions and LCO amplitudes for simply supported $[0/-45/45/90]_s$ plate with SMA, $\Lambda = 0$.

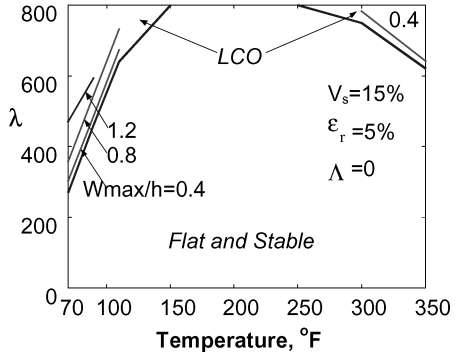

Fig. 13 Stability regions and LCO amplitudes for simply supported $[0/-45/45/90]_s$ plate with SMA, $\Lambda = 0$.

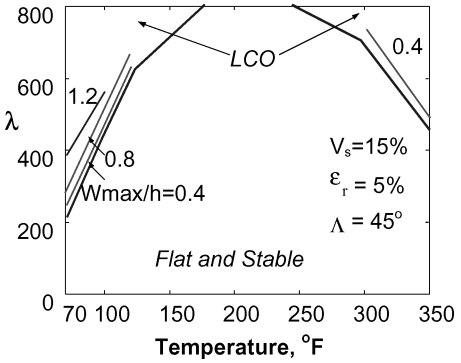

Fig. 14 Stability regions and LCO amplitudes for simply supported $[0/-45/45/90]_s$ plate with SMA, $\Lambda = 45$ deg.

For the SMA embedded composites with $v_s = 10\%$ and $\varepsilon_r = 5\%$, Fig. 12 shows the stability regions at $\Lambda = 0$ ($C_a = 0.05$). Compared with Fig. 10, the buckled but dynamically stable region and the chaos regions are eliminated from the ($T \sim \lambda$) domain investigated and the flat and stable region occupies more than half of the total area. If only v_s is increased from 10 to 15%, the flat and stable region is even larger and occupies most of the domain, as shown in Fig. 13.

Figure 14 shows the stability boundaries at flow yaw angle $\Lambda = 45$ deg. It gives a slightly smaller flat and stable region as compared with $\Lambda = 0$ in Fig. 13. This indicates that flow yaw angle is an important parameter for flutter suppression investigations.

Conclusions

Aerothermal postbuckling and flutter of composite panels with and without SMA at elevated temperatures are investigated. The finite element formulations and the solution procedures in conjunction

with the IUL method for nonlinear temperature-dependent material properties of SMA are presented. The stability boundaries of composite plates with various SMA volume fractions and prestrains are studied. Results showed that the critical temperature could be raised high enough so that postbuckling deflection can be eliminated and the flat and stable region for flutter can be enlarged greatly for supersonic vehicle applications. Results also show that the zero flow yaw angle is not the worst case in stability boundary for general composite panels. Weight calculations based on critical temperature also showed that SMA greatly reduces the weight as compared with traditional composite and titanium surface panels.

References

[1]Wilson, J. R., "The New Shape of Supersonics," *Aerospace America*, June 2002, pp. 26–33.

[2]Chen, R., and Blosser, M., "Metallic Thermal Protection System Panel Flutter Study," AIAA Paper 2002-0501, Jan. 2002.

[3]Cheng, G., Mei, C., and Chen, R. R., "Methodology for Supersonic Panel Flutter Analysis of Thermal Protection System," *Journal of Aircraft*, Vol. 38, No. 6, 2001, pp. 1025–1031.

[4]Buehler, W. J., and Wang, F. E., "A Summary of Recent Research on the Nitinol Alloys and Their Potential Applications in Ocean Engineering," *Ocean Engineering*, Vol. 1, No. 1, 1968, pp. 105–120.

[5]Cross, W. B., Kariotis, A. H., and Stimler, F. J., "Nitinol Characterization Study," NASA CR-1433, Sept. 1969.

[6]Baz, A., Ro, J., Mutta, M., and Gilheany, J., "Active Control of Nitinol-Reinforced Composite Beams," *Active Materials and Adaptive Structures*, IOP Publishing, Ltd., London, 1992, pp. 167–176.

[7]Baz, A., Poh, S., Ro, J., Mutta, M., and Gilheany, J., "Active Control of Nitinol-Reinforced Composite Beam," *Intelligent Structural Systems*, Kluwer Academic, Dordrecht, The Netherlands, 1992, pp. 169–212.

[8]Rogers, C. A., "Novel Design Concepts Utilizing Shape Memory Alloy Reinforced Composite," *Proceedings of 3rd Technology Conference of American Society for Composites*, Technomic, Lancaster, PA, 1988, pp. 719–731.

[9]Schrooten, J., Michaud, V. J., Zhang, Y., Balta-Neumann, J. A., and Manson, J. E., "Shape Memory Alloy Wires Turn Composites into Smart Structures Part I: Material Requirements," *SPIE Proceedings of Smart Structures and Materials*, edited by A. R. McGowan, Vol. 4698, Society of Photo-Optical Instrumentation Engineers (International Society for Optical Engineering), Bellingham, WA, 2002, pp. 395–405.

[10]Michaud, V. J., Schrooten, J., Zhang, Y., Parlinska, M. G. F., and Bidaux, J. E., "Shape Memory Alloy Wires Turn Composites into Smart Structures Part II: Manufacturing and Properties," *SPIE Proceedings of Smart Structures and Materials*, edited by A. R. McGowan, Vol. 4698, Society of Photo-Optical Instrumentation Engineers (International Society for Optical Engineering), Bellingham, WA, 2002, pp. 406–415.

[11]Turner, T. L., "Dynamic Response Tuning of Composite Beams by Embedded Shape Memory Alloy Actuators," *SPIE Proceedings of Smart Structures and Materials*, edited by J. H. Jacobs, Vol. 3991, Society of Photo-Optical Instrumentation Engineers (International Society for Optical Engineering), Bellingham, WA, 2000, pp. 377–388.

[12]Turner, T. L., "Thermomechanical Response of Shape Memory Alloy Hybrid Composites," NASA TM-2001-210656, NASA Langley Research Center, Jan. 2001.

[13]Thornton, E. A., "Thermal Buckling of Plates and Shells," *Applied Mechanics Reviews*, Vol. 46, No. 10, 1993, pp. 485–506.

[14]Noor, A. K., and Burton, W. S., "Computation Models for High-Temperature Multilayered Composite Plates and Shells," *Applied Mechanics Reviews*, Vol. 45, No. 10, 1992, pp. 419–446.

[15]Kamiya, N., and Fukui, A., "Finite Deflection and Postbuckling Behavior of Heated Rectangular Plates with Temperature-Dependent Properties," *Nuclear Engineering and Design*, Vol. 72, No. 3, 1982, pp. 415–420.

[16]Chen, L. W., and Chen, L. Y., "Thermal Buckling Behavior of Laminated Composite Plates with Temperature-Dependent Properties," *Composite Structures*, Vol. 13, No. 4, 1989, pp. 275–287.

[17]Chen, L. W., and Chen, L. Y., "Thermal Postbuckling Behavior of Laminated Composite Plates with Temperature-Dependent Properties," *Composite Structures*, Vol. 19, No. 3, 1991, pp. 267–283.

[18]Noor, A. K., and Burton, W. S., "Three-Dimensional Solutions for the Thermal Buckling and Sensitivity Derivatives of Temperature-Sensitive Multilayered Angle-Ply Plates," *Journal of Applied Mechanics*, Vol. 59, No. 10, 1992, pp. 848–856.

[19]Lee, I., Oh, I. K., and Lee, D. M., "Supersonic Flutter Analysis of Stiffened Composite Plate Subject to Thermal Load," *Journal of Sound and Vibration*, Vol. 224, No. 1, 1999, pp. 49–67.

[20]Mei, C., Duan, B., and Zhong, Z. W., "Large Thermal Deflections of Composite Plates with Temperature Dependent Properties," U.S. Air Force Weapons Lab., Rept. AFWL-VA-WP-TR-1999-3036, Wright–Patterson AFB, OH, Feb. 1999.

[21]Duan, B., Tawfik, M., Goek, S. N., Ro, J.-J., and Mei, C., "Analysis and Control of Large Thermal Deflection of Composite Plates Using Shape Memory Alloy," *SPIE Proceedings of Smart Structures and Materials*, Vol. 3991, Society of Photo-Optical Instrumentation Engineers (International Society for Optical Engineering), Bellingham, WA, 2000, pp. 358–365.

[22]Duan, B., "Suppression of Composite Panel Vibration Under Combined Aerodynamic and Acoustic Excitation at Elevated Temperatures Using Shape Memory Alloy," Ph.D. Dissertation, Dept. of Aerospace Engineering, Old Dominion Univ., Norfolk, VA, May 2001, pp. 70–101.

[23]Dowell, E. H., "Observation and Evolution of Chaos for an Autonomous System," *Journal of Applied Mechanics*, Vol. 51, No. 3, 1984, pp. 664–673.

[24]Mei, C., Abdel-Motagaly, K., and Chen, R., "Review of Nonlinear Panel Flutter at Supersonic and Hypersonic Speeds," *Applied Mechanics Reviews*, Vol. 52, No. 19, 1999, pp. 321–332.

[25]Selvam, R. P., Qu, Z. Q., and Zheng, Q., "Three-Dimensional Nonlinear Panel Flutter at Supersonic Euler Flow," AIAA Paper 2002-1485, April 2002.

[26]Friedmann, P., and Hanin, M., "Supersonic Nonlinear Flutter of Orthotropic or Isotropic Panels with Arbitrary Flow Direction," *Israel Journal Technology*, Vol. 6, No. 1-2, 1968, pp. 46–57.

[27]Chandiramani, N. K., Plaut, R. H., and Librescu, L., "Nonperiodic Flutter of a Buckled Composite Panel," *Sadhana Journal*, Vol. 20, Pts. 2–4, April–Aug. 1995, pp. 671–689.

[28]Chandiramani, N. K., Plaut, R. H., and Librescu, L., "Nonlinear Flutter of Buckled Shear-Deformable Composite Panel in a High Supersonic Flow," *Journal of Nonlinear Mechanics*, Vol. 30, No. 2, 1995, pp. 149–167.

[29]Abdel-Motagaly, K., Chen, R., and Mei, C., "Nonlinear Flutter of Composite Panels Under Yawed Supersonic Flow Using Finite Elements," *AIAA Journal*, Vol. 37, No. 9, 1999, pp. 1025–1032.

[30]Mei, C., Dhainaut, J. M., Duan, B., Spottswood, S. M., and Wolfe, H. F., "Nonlinear Random Response of Composite Panels in an Elevated Thermal Environment," U.S. Air Force Research Lab., Rept. AFRL-VA-WP-TR-2000-3049, Wright–Patterson AFB, OH, Oct. 2000.

[31]Bogner, F. K., Fox, R. L., and Schmit, L. A., "The Generation of Inter-Element Compatible Stiffness and Mass Matrices by the Use of Interpolation Formulas," U.S. Air Force Flight Dynamics Lab., Rept. AFFDL-TR-66-80, Wright–Patterson AFB, OH, 1966, pp. 396–443.

C. Pierre
Associate Editor